PAPER

Check for updates

Intestines of non-uniform stiffness mold the corners of wombat feces†

Patricia J. Yang,‡[a] Alexander B. Lee,‡[b] Miles Chan,[a] Michael Kowalski,[c] Kelly Qiu,[c] Christopher Waid,[c] Gabriel Cervantes,[a] Benjamin Magondu,[c] Morgan Biagioni,[a] Larry Vogelnest,[d] Alynn Martin,[e] Ashley Edwards,[e] Scott Carver*[e] and David L. Hu [ID] *[ab]

The bare-nosed wombat (*Vombatus ursinus*) is a fossorial, herbivorous, Australian marsupial, renowned for its cubic feces. However, the ability of the wombat's soft intestine to sculpt flat faces and sharp corners in feces is poorly understood. In this combined experimental and numerical study, we show one mechanism for the formation of corners in a highly damped environment. Wombat dissections show that cubes are formed within the last 17 percent of the intestine. Using histology and tensile testing, we discover that the cross-section of the intestine exhibits regions with a two-fold increase in thickness and a four-fold increase in stiffness, which we hypothesize facilitates the formation of corners by contractions of the intestine. Using a mathematical model, we simulate a series of azimuthal contractions of a damped elastic ring composed of alternating stiff and soft regions. Increased stiffness ratio and higher Reynolds number yield shapes that are more square. The corners arise from faster contraction in the stiff regions and relatively slower movement in the center of the soft regions. These results may have applications in manufacturing, clinical pathology, and digestive health.

1 Introduction

The ability of wombats to form relatively uniform, clean cut, cubic feces – as opposed to the tapered cylindrical feces of most animals – is unique in the animal kingdom. The earliest documented observation of wombat cubic feces is by Eric Guiler (1960), who states: "The droppings of wombats are of a characteristic rectangular shape".[1] The next publication dates 1979,[2] although the droppings were known within Australia well prior to both these references. It is currently poorly understood how these animals produce geometric scats. With no immediately apparent explanation as to how an animal's defecation process could produce cube-shaped scats, a range of hypotheses have been proposed over decades.[3–5] A sample of hypotheses include compression of fecal material between pelvic bones, a relatively geometric-shaped sphincter, and parallel blocks of longitudinal intestinal smooth muscles in the cecum. Notably, all hypotheses have exclusively remained the matter of objective speculation and assumed mechanism, rather than subject to actual investigation.

The ability of wombats to form cubic feces is of both general and practical interest. How animals engage in varying forms of communication, and the underlying evolutionary forces driving them, have been of interest to ecologists for decades. Recent fluid dynamic modelling has investigated cylindrical scat formation,[6] with clinical application to diarrhea and constipation disorders,[7] however mechanisms leading to the formation of diverse fecal shapes is less understood. In the built world, cubes and shapes with sharp edges are made by cutting, molding or extrusion. Examples include extruded pasta, hay cubes and injection-moulded plastics. Cube formation in animal models appears to be a new method, and may inform manufacturing processes, particularly if soft biological materials are of interest. Another application may be in the care of captive animals. In Australia, wombats are kept in captivity in zoos and wildlife parks, and their feces are cleared on a daily basis. Quantifying a wombat's scat shape may be a useful metric for non-invasively assessing the quality of a wombat's diet, digestive health, or level of hydration.

The spontaneous formation of geometric structures has long been the purview of a field of physics called pattern formation.

[a] *School of Mechanical Engineering, Georgia Institute of Technology, 801 Ferst Drive, MRDC 1308, Atlanta, GA 30332, USA. E-mail: hu@me.gatech.edu; Tel: +1 404 894-0573*

[b] *School of Biological Science, Georgia Institute of Technology, 801 Ferst Drive, MRDC 1308, Atlanta, GA 30332, USA*

[c] *School of Biomedical Engineering, Georgia Institute of Technology, 801 Ferst Drive, MRDC 1308, Atlanta, GA 30332, USA*

[d] *Taronga Conservation Society, Mosman, NSW 2088, Australia*

[e] *Department of Biological Science, University of Tasmania, Hobart, Tasmania 7005, Australia. E-mail: scott.carver@utas.edu.au; Tel: +61 3 6226 2794*

‡ Co-first author.

Geometric patterns have been observed in geology, physics, and biology. The processes of cooling lava at Giant's Causeway Ireland or of drying cornstarch leads to hexagonal columns called columnar jointings.[8] Since the 1800s it has been known that vibration of a membrane generates beautiful arrangements of grains of sand known as Chladni figures.[9] This is due to nodal lines being created between parts of the plate that vibrate in opposite directions. When a central stream of water strikes a kitchen sink, a roughly circular standing wave of fluid is created, but when the fluid is viscous, polygons such as two, three, four, and five sided shapes can be observed.[10,11] In biology, pattern formation is responsible for the wing venation patterns of dragonflies[12] and the formation of toothed gears in certain jumping insects.[13] Despite the ubiquity of these patterns, squares are rare, and cubes even more so.

In this study, we will focus on the bare-nosed wombat *Vombatus ursinus*, which produces the most cubic feces of the three species of wombat. The bare-nosed wombat, shown in Fig. 1a, has an adult body length 1 m and mass 20–35 kg. It is drought-tolerant and lives a solitary lifestyle in underground burrows. It typically produces 80–100 cubic feces per day mostly above ground.[3] Wombats generally have low-nutrient diets, primarily consisting of grasses and sedges.[14] To compensate, they have long, spacious intestines of length 6–9 m (see Fig. 1d), utilize hind-gut fermentation, and have a mean food passage retention time of 40–80 h.[14,15] In comparison, a human of 100 kg has an intestinal length of 8 m, fore-gut fermentation, and a mean food passage retention time of 50 h.[16,17] The extended digestion period of wombats allows them to maintain exceptionally low metabolic rates[18,19] and also an energetically expensive digging lifestyle.[20] These attributes allow the wombat to survive droughts that would challenge most other mammals.

Animals have long been known for using their urine and feces to communicate. However, wombats have a unique way of using their feces as markings. Wombats, particularly bare-nosed wombats, have a propensity to deposit feces in aggregations called latrines. Such latrines are found on or next to distinctive landscape features such as prominent rocks, logs and small rises, and burrow entrances within their home ranges,[3,21] as shown in Fig. 1b. Latrines are generally found with five or more wombat scats indicating that one or several wombats may be involved. It is generally believed that prominent latrines facilitate visual or olfactory communication between wombats or other nearby animals. It has been proposed that the flat sides of the feces serves the purpose of latrine stability by preventing the feces from rolling off these raised surfaces.[3–5] Understanding how wombats produce cubes may provide insight into how such a unique adaptation evolved.

In this study we investigate cube formation in the wombat using dissections, material measurements, and mathematical modeling. We begin in Section 2 with the histological and tensile experiments performed on wombat intestine samples as well as 2D phenomenological modeling informed by these experiments. In Section 3, we discuss the implications of our work and provide suggestions for future research. In Section 4, we summarize the contributions of our study. In Section 5, we provide the detailed methods.

2 Results

2.1 Wombat experiments

If wombats were to make cubes similar to the way we make noodles, we would expect a square anal sphincter. In 2019, we obtain a CT scan of a live adult female wombat (Video S1, ESI†). The scan shows that the wombat's anus is round, a feature consistent with all other animals. Also, the pelvic bones, which the feces were once proposed to glide past, are nowhere in the vicinity of the colon. We thus conclude that wombats do not change their feces shape through extrusion. We obtain further evidence that extrusion does not influence shape with a series of dissections of wombats.

In this study, we present data from three dissected wombats, all obtained following euthanasia by veterinarian owing to vehicle collisions in 2018–2020. Unfortunately, vehicle collisions are a source of wombat and other marsupial mortality events in Australia. In 2018, we dissect a young female wombat (2–3 years old). In 2019, we dissect an adult male wombat (>2 years old). And in 2020, we dissect a young male wombat (<2 years old). Given the similarity in age and size of all wombats, we expect feces and intestinal measurements to be comparable. All dissected wombats are referred to by the year of dissection. From the 2018 wombat, cubic feces are removed from the end of the distal colon and unformed feces removed from the end of the proximal colon. One of the cubic feces is scanned with
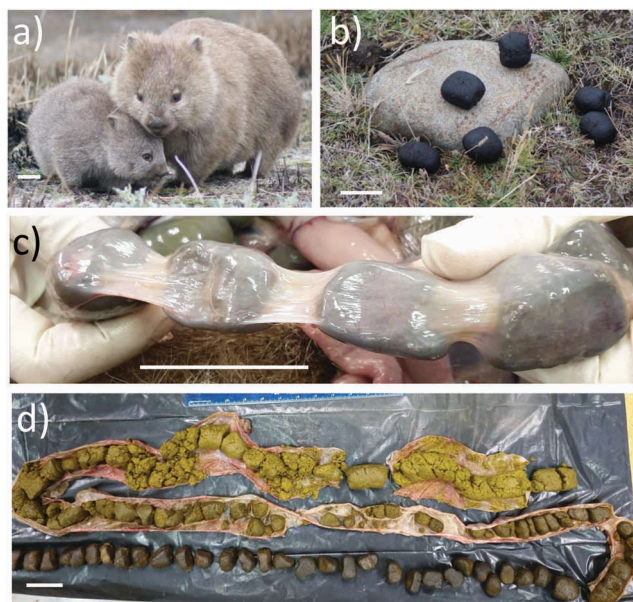
Fig. 1 Wombats form cubic feces. All scalebars represent 5 cm. (a) A female wombat with her joey. (b) A typical wombat latrine consisting of feces placed on a low rock or stump. (c) A 2019 dissection of a wombat shows the cubic feces fully formed within the mid-distal colon, (d) the excised 3 m of wombat intestine shows feces transforming from a yellow yogurt-like slurry near the stomach to darkened dry cubes near the anus.

a Faro arm to obtain a 3D point cloud reconstruction (see Video S2, ESI†).

The wombat intestine of 6–9 m length (approximate length for a fully grown wombat) consists of four sections after the oesophagus: these include the stomach (0.14 m), a relatively short small intestine (3.2 m), long proximal colon (3.9 m) and distal colon (last 1.8 m). Fig. 1d shows the shape of feces with relation to their position in the intestine (lower proximal colon to lower distal colon). In the proximal colon, the feces are a yellow-green slurry of digesta. As the fecal material approaches the anus, it becomes increasingly dry, as shown by the darker color. The beveled edges and flat faces also become increasingly prominent.

The removal of water from the feces may help it to better retain its shape. Generally, at higher solid fractions, mammalian feces are more viscous and behave viscoplastically.[22] To measure the level of dryness we begin by removing feces samples from both the proximal and distal colons. By weighing a scat, we obtain m_{wet}, and by drying them in an oven, we obtain m_{dry}. We define the water content of each sample using $w = \dfrac{m_{wet} - m_{dry}}{m_{wet}}$. Feces from the proximal colon have a water content of $w = 0.81$ and show an amorphous shape. Feces from the distal colon, the last 1 m (or 17 percent) of the 6 m digestive tract, have a much lower water content of $w = 0.53$. This water content is lower than many mammals: for example, humans have a fecal water content of $w = 0.74$.[23]

The fecal cubes have dimensions: height 2.3 ± 0.3 cm, width 2.5 ± 0.3 cm, and axial length 4.0 ± 0.6 cm (see Fig. 2), and the edges of the feces are beveled. Thus, the aspect ratio of the feces is $1:1:1.6$, and so technically the feces are rectangular prisms, but for simplicity, we continue to refer to them as cubes in this paper.

To understand the formation of the cubes, we hang an intact intestine vertically allowing the bottom end to swing and rotate freely. We observe that the corners of the cubes are aligned, suggesting that the intestine itself has a coordinate system to dictate corner formation. We hypothesize that this coordinate system is written in the intestines in terms of its thickness and its material properties. To explore this idea, we turn to histology and material testing.

2.2 Material properties of wombat intestine

From the 2019 wombat, two cross sections of the intestines are hematoxylin and eosin stained and the thickness of the tissue layers are measured under a microscope. Since the cubes form in the distal colon, and are amorphous in the proximal colon, we obtain cross sections from both the proximal and distal colon and perform histological staining. These sections are 50 cm and 200 cm away from the anus. We observe the four major tissue layers, arranged external to internal: longitudinal muscle, circular muscle, glandular tissue, and mucosa, as labelled in Fig. 3a and b with the letters L, C, G, M, respectively. In particular, the circular and longitudinal muscle thickness varies greatly between different azimuthal locations, and so we focus on these two layers from hereon.
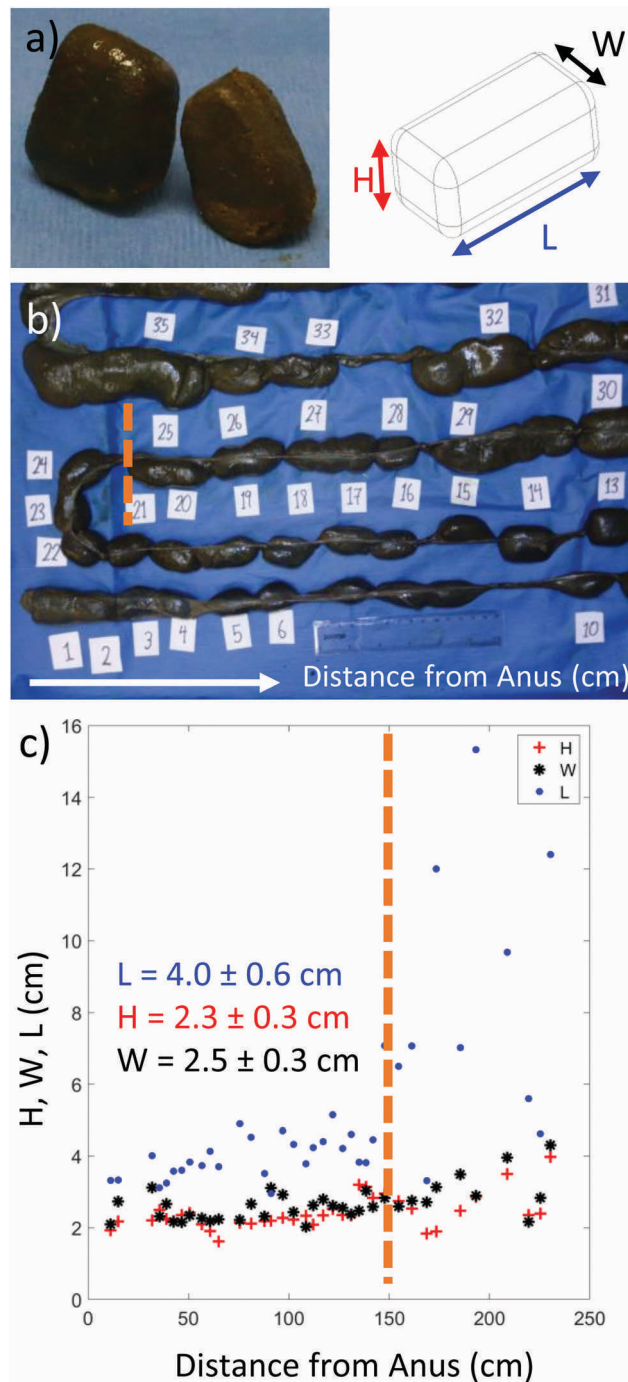

Fig. 2 Wombat feces within intact intestines. (a) Two wombat fecal pellets and schematic showing the length, height, and width of each pellet. (b) Figure of preserved wombat intestines spread out to show the natural progression towards cube-shaped. The feces labeled 1 is at the anus. The orange dotted line marks 1.5 m from the anus. (c) The relationship between wombat feces length scale and distance from the anus. The last 1.5 m shows consistent dimensions of $4 \times 2.3 \times 2.5$ cm.

Fig. 3c and d shows the relationship between tissue thickness and azimuthal position in the proximal and distal colon. We arbitrarily assign $\theta = 0°$ as the position of observed lowest thickness of the intestine. The longitudinal muscle, the circular muscle, and the total thickness of both muscles are shown by
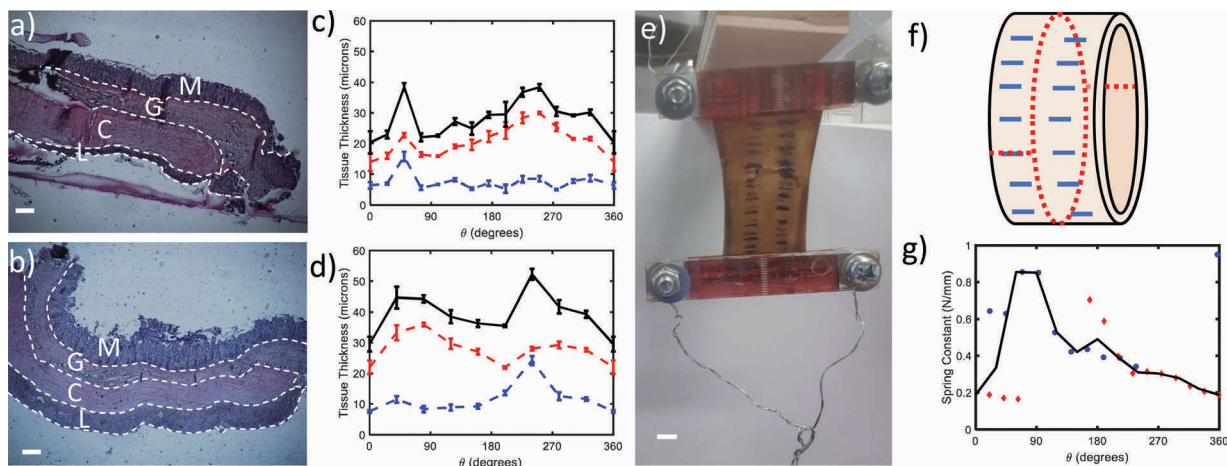
Fig. 3 Non-uniform thickness and stiffness of the wombat intestine. (a and b) Histology of the distal colon, with the longitudinal muscle, circular muscle, glandular tissue, and mucosa layer labelled with the letters L, C, G, M, respectively. Scale bar, 20 microns. (a) Staining corresponds to the azimuthal position $\theta = 40°$ and shows the thinnest longitudinal muscle thickness. (b) Staining corresponds to $\theta = 240°$ and shows the largest longitudinal thickness. (c and d) The relationship between azimuthal position and tissue thickness, with the longitudinal muscle, circular muscle and total muscle thickness given by the blue, red, and black lines, respectively. (c) is from the proximal colon, and (d) from the distal colon. (e) Custom-built tensile testing setup for the wombat intestines. Scalebar, 1 cm. (f) Schematic showing two sequential cross sections cut at 180° offset to obtain tensile testing data of the full 360°. Cuts are made at the dotted red lines and tick marks are drawn using the blue lines. (g) The relationship between azimuthal position and tissue stiffness. The blue and red points correspond to each of the adjacent cross sections and the black line to the average stiffness.

the blue, red, and black lines, respectively. Examining the distal colon section first, shown in Fig. 3d, the longitudinal tissue layer more than doubles in thickness, from 10 μm to 25 μm, with the peak occurring at $\theta = 240°$. The circular muscle also has a 50% increase from 22 μm to 35 μm, with peak at $\theta = 90°$. It is noteworthy that the peaks are 180° out of phase, as shown by the the total thickness, which has peaks at around 90° and 270°.

As shown in Fig. 3c, the proximal colon also has two peaks. The azimuthal location may not match that of the distal colon because we could not maintain azimuthal alignment between the two sections. The presence of thickness peaks combined with the absence of the cubic feces in the proximal region indicates to us that both feces dryness and axisymmetric intestinal properties must be present to enable cubing to occur.

From the 2020 wombat we test the tensile material properties to determine the effects of non-uniform tissue thickness. We cut two sequential cross sections of the distal colon to perform material testing. These circular bands are cut 180° out of phase so that we can obtain data in regions that have been clamped during the testing (see Fig. 3e and f). We perform tensile testing to measure stiffness as a function of azimuthal position. We infer stiffness by the strain measured between lines drawn at increments of 4 mm. Fig. 3g shows the relationship between stiffness and azimuthal position, where the blue and red points are stiffness from each of the two cross sections, and the black is the average stiffness of each 30° region. We observe a single peak in stiffness at $\theta = 90°$ in the distal colon, where $\theta = 0°$ is set to be the location of lowest stiffness. Because the two cross sections are sequential we expect them to have comparable trends. Wide discrepancies in the data near $\theta = 0°$ and at $\theta = 180°$ are likely due to the tissue being clamped near those regions, which affects its ability to stretch laterally, affecting the stiffness measurement.

2.3 Simulation of intestinal contractions

We continue with our study using a theoretical model that assumes that there are two bands of increased stiffness located 180° out of phase. Tensile testing of passive tissue only displays a single stiff region, but this test only measures azimuthal stretching. A peristaltic contraction relies upon muscles in both the azimuthal and the longitudinal directions. We surmise that the peak in stiffness observed in the tensile test may correspond to the factor of three increased thickness in the longitudinal muscle. The 0.5 factor of increased thickness in the circular muscle apparently was not detected by our tensile test. We hypothesize that the increased circular muscle thickness results in a locally stronger muscle contraction during peristalsis. This locally increased contraction would phenomenologically be similar to an increased stiffness. For simplicity, we develop our model as having two stiff regions to represent the increased thickness of longitudinal and circular muscles. An important parameter in this model is the stiffness ratio C, the ratio between maximum and minimum stiffness, which we observe in our tensile tests to be 4 (see Fig. 3g, peak stiffness is 4 times that of baseline stiffness).

We propose a phenonemological model to investigate how non-uniform intestinal properties can influence feces shape during peristaltic contractions. The goal of our model is to rationalize how two regions of stiffness can result in four corners of the feces. A square is defined as having 8 regions of differing curvature: zero curvature at the flat sides, and steep peaks at each of the corners. It is thus not obvious how the contraction of a band with 2 regions of stiffness can result in 4 peaks in curvature.

We begin with a few caveats on our model. The real wombat intestines are three-dimensional and filled with viscoelastic

feces. The peristaltic contractions occur at an unknown intensity for an unknown duration. Thus, a fully accurate three-dimensional model cannot be done with the current knowledge about the intestine material dynamics. Instead, we take a simplified approach: our model is two dimensional, considering a circular cross-section of the intestine. Rather than modeling the interaction between the intestines and the viscoelastic feces, the feces are represented as added mass along the intestinal walls as well as a linear damping in all directions.

We conduct our modeling in two phases, beginning with an equilibrium phase to create an initial strained state of the intestine, and followed by a non-equilibrium series of contractions. In the first phase, feces are initially pushed into the 2D cross-section of our model. We assume the feces exerts a constant pressure against the intestinal walls until the system comes to equilibrium. We find that this equilibrium state is necessary to prevent unphysical behavior in the second phase of the model.

Once the initial equilibrium state of strain is found, the intestine begins contracting by shortening the springs' rest length, l_0. Multiple contractions are simulated by changing the rest length to a contracted value, holding the contraction, and then taking a relaxed value, and holding this length. The contraction dynamics are thus idealized as a square wave. The governing equations arise from the damping force in all directions and the elastic spring forces of the intestinal walls.

The evolution of the solution shape is recorded as a function of time. Since the wombat fecal pellet changes shape as it travels down the intestine over 2–4 days, it is not clear whether it reaches an equilibrium shape before it is ejected. Thus, our goal is not to find an equilibrium shape for the feces but to record how transient square-like shapes can arise. We also use this method to determine how different intestinal and fecal parameters may influence the shape.

Now that we have discussed the general idea of the model, we turn to the specifics of the implementation. We divide the intestine into a ring of $4n$ nodes, each of mass m. Each node is connected to its neighboring nodes using linear springs of varying stiffness. We divide the ring into 4 quadrants of n nodes each. The regions are sequentially soft and stiff in an alternating ABAB pattern, shown in Fig. 4a, and similar to the variation in thickness we observe from the wombat histology. The soft zones have springs of stiffness $4nk$, and the stiff zones have stiffness of $4Cnk$, where the stiffness ratio $C > 1$. Including n as a factor in the stiffness allows the overall stiffness of the system to be independent of the number of nodes in the ring.

To find the initial configuration for the model, we solve for the equilibrium state. This state will depend on the minimum and maximum spring stiffness $4nk$ and $4Cnk$, and the spring lengths l_i. It does not depend on mass or damping, which arise in the contraction phase. As the feces is pushed into the 2D intestinal ring, it exerts an outward constant pressure P.
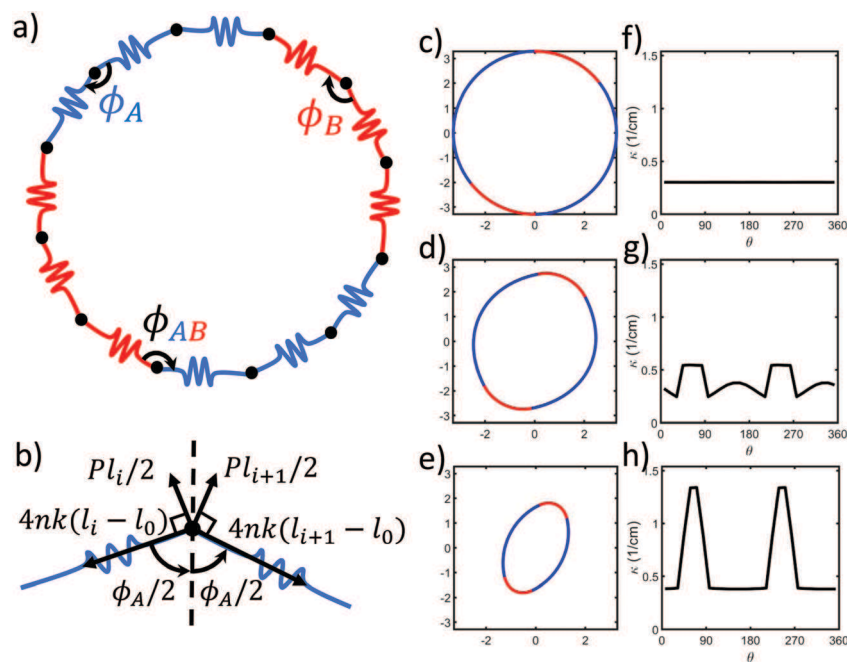
Fig. 4 The mathematical model of contracting wombat intestines. (a) Schematic of the elastic ring simulating the intestine. Blue and red regions indicate low and high stiffness zones, respectively. This color scheme is valid for (c–e) as well. (b) Close-up of the variables defined at a single node. The equilibrium shape of the intestine arises from solving the force balances perpendicular and parallel to the angular bisector shown. (c–e) Sequence of intestine shapes during a series of contractions and the corresponding relationships (f–h) between curvature and azimuthal positions for each of these shapes. For these simulations, $C = 4$, and Re = 10^{-3}. (c) At time $t = 0$ s, the equilibrium shape is close to circular, and the curvature (f) is near constant. (d) After several contractions, the intestine becomes increasingly square ($t = 7.9$ s), as shown. Note that depending on the Reynolds number and stiffness, some shapes are more square than others. The four peaks of curvature in (g) correspond to the four corners. (e) Past the peak squareness, S, the contraction continues to deform the intestine, and the shape begins to resemble an ellipse. This frame corresponds to a time $t = 30$ s.

The equilibrium arrangement of nodes is found from the local force balance on the individual nodes. Consider a node within the soft region (see Fig. 4b). Attached to it are two springs of stiffness $4nk$, stretched to lengths l_1 and l_2, respectively. The angle formed between the springs is ϕ. The pressure force exerted on the node is perpendicular to the spring and proportional to the spring length, $\frac{1}{2}Pl_1$ and $\frac{1}{2}Pl_2$. We draw our axis parallel and perpendicular to the angular bisector. By considering the force balance perpendicular to the angular bisector, we see that $l_1 = l_2$. This also holds true for nodes within the stiff region. We can also show that if all of the spring lengths are the same, the angle ϕ of each of those nodes must also be the same.

We then have 5 unknowns: l_A and ϕ_A for the soft regions, l_B and ϕ_B for the stiff regions, and ϕ_{AB}, the angle at the 4 interfacial nodes between the stiff and soft regions. We therefore require 5 equations. Four equations come from local force balances, and the final equation comes from the assumed convex geometry of the equilibrium shape. This calculation is described in more detail in Section 5.

The equilibrium shape is used as the initial condition of the intestine before the contraction begins. The contraction of the intestinal wall is simulated by alternating the rest length of each spring from l_0 to $l_0/4$ using a square wave with period τ. As wombat intestine contractions occur at an unknown intensity and period, these parameters were chosen arbitrarily.

$$l_0 = \begin{cases} l_0 & \cos(2\pi t/\tau) < 0 \\ l_0/4 & \cos(2\pi t/\tau) \geq 0 \end{cases} \qquad (1)$$

The net force comes from the two spring forces attached to each node and a damping force $-b\vec{v}_i$ opposing the direction of motion, where b is a damping coefficient and $\vec{v}_i$ is the velocity of the ith node. The mass of each node, m accounts not only for the mass of the intestinal tissue, which is likely negligible, but also the added mass of the feces as it is displaced along the digestive tract.

Fig. 4c–e shows the progression of wombat feces shape during a series of contractions, using $n = 50$ nodes for each region, a stiffness ratio $C = 4$, damping $b = 45$ g s^{-1}, and added mass $m = 0.045$ g. Fig. 4f–h shows the curvature measured around the feces. The initial equilibrium shape of the intestine is fairly circular, as shown by the nearly constant curvature in Fig. 4f. Fig. 4d shows the peak squareness during mid-contraction, where the feces shows the start of 4 corners, and the curvature in Fig. 4g shows 4 peaks. The intestine displays this transient square state and then passes out of the square state as the contractions continue. We show a point later in the contractions in Fig. 4e and h showing the feces is clearly less square.

2.4 Simulation analysis

While it is easy to qualitatively distinguish between circles and squares in both the simulation shape and the curvature, $\kappa(\theta)$, graphs, we require a way to quantitatively measure the squareness of the shape. There exist many simple methods to measure

how round an object is,[24] and we find one potential way to measure squareness based on the definition of the squircle.[25] However, the method based on the squircle definition is not robust to the noise found when applied to natural wombat feces. It evaluates most samples as very square, but for a few, visually similar samples, it evaluates them as very round (see Supplemental material S1, ESI†).

We proceed by proposing a squareness metric that employs the $\kappa(\theta)$ signal and cross-correlates it to idealized reference curvatures going from the flat curvature of a circle to the infinitely peaked curvature of a square (see Fig. 5a). Our final squareness S is defined in eqn (17) in the Methods section, and varies between 0 and 1, with 1 as being most square.

Fig. 5b shows the time course of feces squareness during the simulation. We perform 40 sequential contractions, with each oscillation in the figure marking a contraction. The squareness has a sharp increase at $t \approx 5$ s with a peak squareness of $S = 0.3$ at $t = 7.9$ s. Subsequently, the squareness decreases, demonstrating the transient nature of the square shape in the simulation.

To determine if our simulation captures the squareness of actual wombat feces, Fig. 5c shows 36 wombat feces collected around Maria Island, off of Tasmania, Australia. A histogram of the squareness of these samples is shown in Fig. 5d, and we find that the feces have a mean squareness of 0.14 with a standard deviation of 0.1. These lower values appear to be due to sensitivity to the shape's aspect ratio. For rectangular shapes, the corners are not spaced apart azimuthally in a way that matches the reference curvature. Nevertheless, our metric gives similar values to visually similar shapes. We proceed by using our squareness metric to explore the effect that different simulation parameters have on the resulting feces shape.

We consider two dimensionless groups as the independent variables that characterize the intestinal contraction: the stiffness ratio C, and the Reynolds number, Re. The stiffness ratio is defined as

$$C = \frac{\text{stiffness of stiff region}}{\text{stiffness of soft region}}, \qquad (2)$$

where we observe wombat feces has a stiffness ratio of $C = 4$. We conduct simulations by matching simulation Reynolds number Re with the biological Reynolds number Re_b, defined as

$$Re_b = \frac{\rho L v}{\mu} = \frac{\text{inertia}}{\text{viscous force}}, \qquad (3)$$

where ρ and μ are the density and dynamic viscosity of the feces respectively. We focus on the Reynolds number characterizing the peristaltic contractions that generates the square cross section, and not the Reynolds number of the slower axial flow through the intestines. Therefore, L is the radius of the intestine and v is the radial velocity of the intestine during a contraction. For the feces of mammals,[6] $\rho \approx 1$ g cm^{-3} and μ varies between 10^3–10^5 g (cm s)$^{-1}$. The radius of the wombat intestine is on the order of unity, $L \approx 1$ cm. Based on the peristaltic contraction frequency of dogs and humans,[26] which
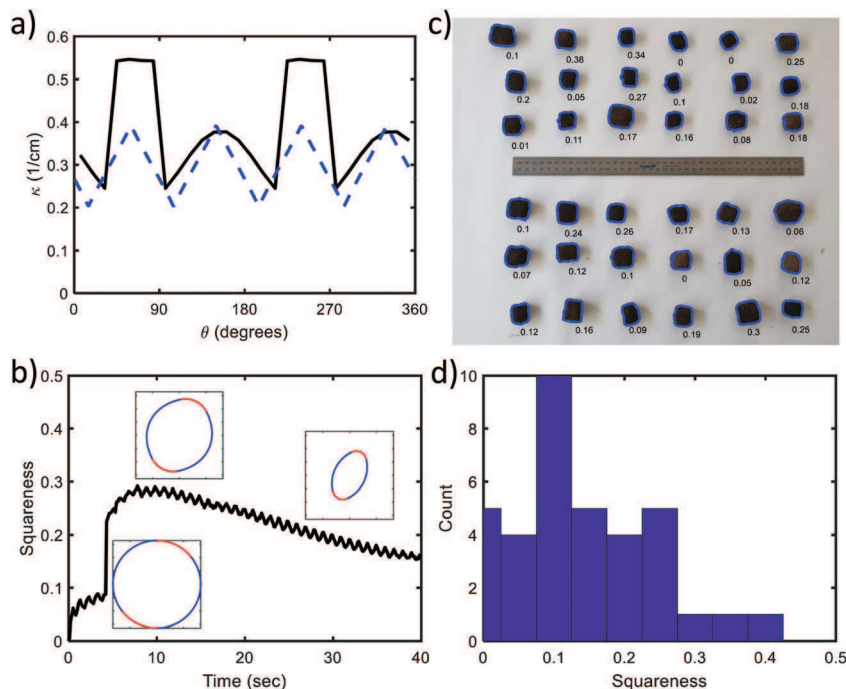
Fig. 5 Squareness for simulated and actual wombat feces. (a) The relationship between curvature and aziumthal position. The curvature at one point in time ($t = 7.9$ s) during a contraction is shown by the black solid line. To evaluate squareness this curvature is correlated to the corresponding reference curvature shown by the blue dotted line. The reference curvature shape is defined using the variable λ. Decreasing λ corresponds to greater peaks in curvature, and greater squareness S. (b) The time course of squareness S during a series of intestinal contractions. Insets show the simulation shape at $t = 0$, 7.9, and 30 s. The oscillations in squareness correspond to each contraction. (c) An array of 36 wombat feces found on Maria Island in Tasmania. The blue outlines indicate the measured shape using image analysis. The numbers below each feces correspond to the calculated squareness. (d) A histogram of squareness of natural wombat feces from part (c), demonstrating a mean squareness of 0.14 and a standard deviation of 0.1.

are between $f = 0.05$–0.2 Hz, we approximate that wombat intestine contractions have a characteristic radial velocity of $v = fL = 0.01$–1 cm s^{-1}. All together, we approximate the Reynolds number of wombat intestines deforming feces to be Re$_b \approx 10^{-7}$–10^{-3}. Since wombat feces is drier than that of most mammals, the Reynolds number may be even lower, especially near the anus.

Since our simulation is two-dimensional, and only accounts for the feces properties in a phenomenological manner, we must redefine the Reynolds number for the simulation. The length scale is the mean radius of the initial equilibrium intestine configuration, R. Similar to the biological system, the radial velocity is $v = R/\tau$, where τ is the period of the model contractions. Note that the radius, and thus the velocity, are functions of the spring constants, with higher spring constants associated with a smaller equilibrium intestine size. The 2D density is calculated as the added mass divided by the initial area, $\rho_{2D} = m/(\pi R^2)$, which has units of mass per unit area. The viscosity of the feces is quantified by the damping coefficient b, which has units of mass/time. The simulation's Reynolds number is

$$\text{Re} = \frac{\left(m/(\pi R^2)\right) R (R/\tau)}{b} = \frac{m}{\pi b \tau} \qquad (4)$$

To encapsulate the biological Reynolds number, we run simulations in the range of Re = 10^{-4}–10^0. Our first claim is that the two

stiff regions found in the wombat's intestinal tissue serve an important role in forming the transient square state. We investigate this by performing a 1D parameter sweep of the simulation, varying the spring stiffness ratio C, which relates the maximum and minimum stiffness of the intestine, while keeping the Re = 10^{-3}. As C increases, the feces increases in squareness S according to the linear regression $S = 0.02C + 0.2$, $R^2 = 0.98$ (see Fig. 6b). For comparison we include our experimental data by the open symbol, associated with a stiffness ratio $C = 4$ and a squareness $S = 0.14 \pm 0.1$. According to our simulations, this stiffness ratio would yield a squareness of $S = 0.28$, which is twice as large as the field data.

We now use our simulation to address the question of how four peaks in curvature result from only two peaks of stiffness. First consider a uniformly stiff ring. By definition, a smaller circle has higher curvature than a larger circle. Therefore, contracting a uniform ring of springs will naturally cause an increase in curvature.

Now consider contractions of a ring of non-uniform stiffness. In a zone of stiffer springs, an increase in curvature will occur earlier than for zones of softer springs. Since there are two stiff zones, this mechanism leads to two corners forming in the middle of the stiff regions. However, to get the remaining two corners in the correct location, there must be an increase in curvature in the middle of the soft regions as well. We propose that these corners form due to inertial effects at the center of the soft regions. As the stiff regions contract more forcefully, the neighboring nodes of
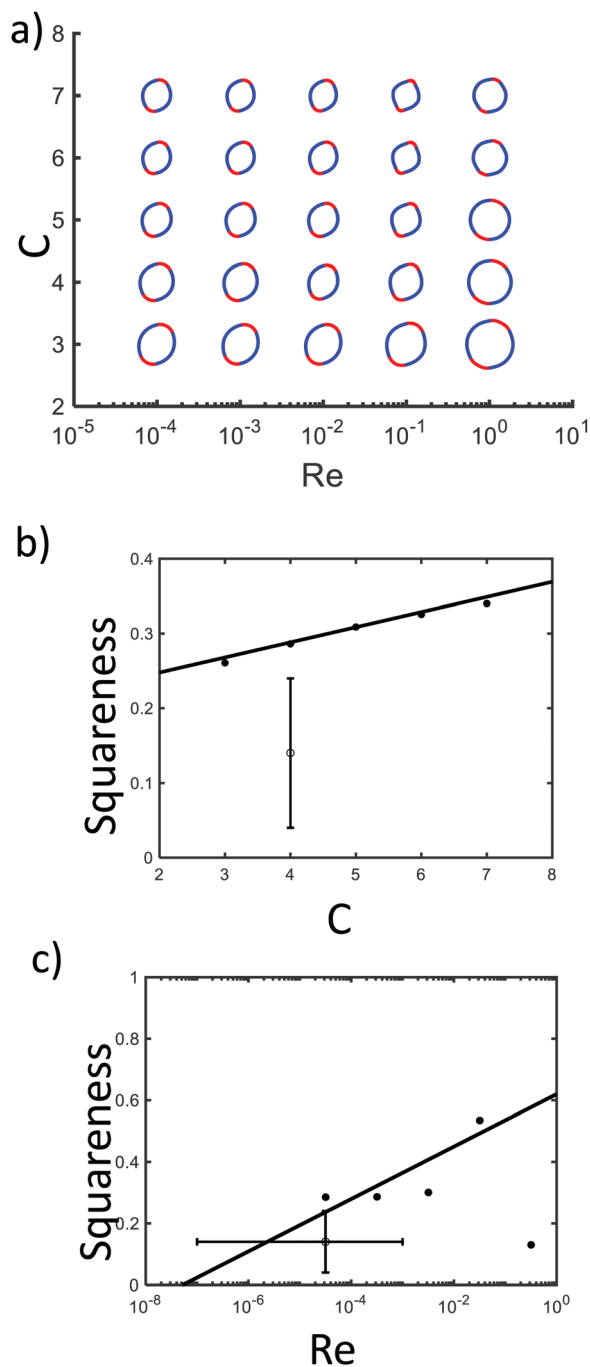
As evidence for this physical picture, we perform a parameter sweep in Reynolds number, shown in Fig. 6c. The stiffness ratio is kept fixed at $C = 4$, and the Reynolds number is varied by manipulating the damping b. As expected, the peak squareness of the simulations increases with Re. The simulation becomes less reliable for Reynolds number approaching 1, due to unphysical behavior such as the intestines crossing itself, which is permitted by the 2D nature of our simulations. Discounting the point at Re near 1, linear regression gives $S = 0.6 + 0.04 \log(\text{Re})$, $R^2 = 0.57$. The simulation show very shallow gains in squareness between Re = 10^{-4}–10^{-2}, but then a significant increase in squareness at Re = 10^{-1}. Fig. 6a shows the full 2D parameter sweep of both the spring stiffness ratio, C, and the Reynolds number. Generally, squareness improves for both higher spring ratios and higher Reynolds number, up to Re = 10^{-1}.

As an additional test of our proposed mechanism for corner formation, we consider the case of three periods of stiffness. With three stiff regions and three soft regions, we expect six corners to form. When running the simulation with three periods of stiffness, we expect a transient hexagon. While the hexagon is barely recognizable, its presence is illustrated by the six peaks in curvature (see Fig. 7). That is to say, if an animal were to evolve 3 or 4 periods of stiffness along the circumference of their intestines, we predict that their feces would take the shape of hexagonal or octagonal prisms.

3 Discussion

In this study, we show that a combination of unique material properties and muscular contractions are necessary for wombats to produce feces with square cross sections. We discover the wombat intestines have non-uniform stiffness along the circumference, in part due to variations in muscle thickness. When intestines conduct their regular peristalsis, digesta is moved towards the anus. Typical peristalsis is uniform in all azimuthal directions because the intestines themselves are uniform. However, the non-uniformity in the wombat intestines cause amplified contractions in distinct pre-set locations. Over many cycles, these non-uniform contractions, along with inertial effects, encourage the preferential movement of feces and the sculpting of the corners. While these inertial effects seem unlikely in a system with such a low Reynolds number, oscillatory motion may cause inertial instabilities at lower-than-expected Reynolds numbers.[27] The flat trend in squareness for simulations at Re = 10^{-4}–10^{-2} suggests that continued reduction of Reynolds number would have negligible effects on the squareness. Multiple contractions of short duration may reduce the magnitude of radial velocities and thus the damping, in comparison to the damping of a single large longer contraction.

Our study shows corners forming in less than 10 contraction cycles. This early corner formation is not realistic because our model does not model the non-Newtonian nature of the feces. With contractions occurring every couple of seconds[26] over a time of 5 days,[15] the feces actually experience on the order of 100 000 contractions. We believe that these missing details may

Fig. 6 Regime diagrams of shape as a function of spring stiffness ratio C and Reynolds number Re. (a) Qualitative 2D sweep of C and Re, showing the peak squareness in the simulation. (b) The relationship between squareness S and spring stiffness ratio C, with solid points given by simulation and line given by linear best fit. The open symbol indicates the squareness of biological wombat feces, with error bars giving the standard deviation in the squareness. (c) The relationship between squareness S and Reynolds number. Solid symbols give the simulation data, and open symbols denote the biological wombat squareness and our estimate for its Reynolds number.

these regions are also dragged towards the center. Conversely, the farthest nodes from the stiff regions are the middle nodes of the soft regions. Their added mass causes them to lag behind, creating an increase in curvature.
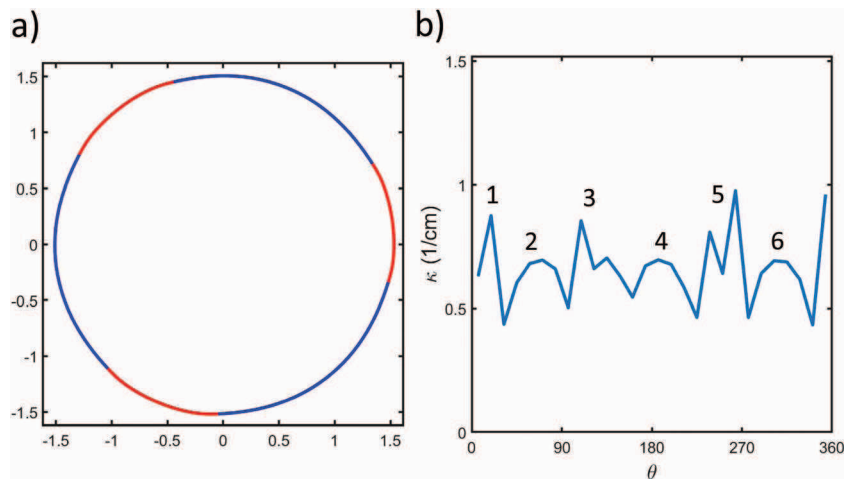
Fig. 7 The results of simulation using 3 stiff regions. (a) A hexagonal feces is formed with barely noticeable corners. (b) The relation between curvature and θ, more clearly showing the six peaks in curvature in part (a).

explain why the model at the lowest Reynolds numbers only shows the initial formation of corners, especially in the soft regions, and why these corners never become sharp. We suspect that as the feces becomes drier, the yield stress nature of the material makes it increasingly capable of holding its cubic shape. Moreover, cubes are found only in the distal colon, and not the proximal colon, despite the periodic tissue thickness found in both regions. Future modeling that takes into account the effects of feces dryness might be able to resolve the onset of cubing in the distal colon.

In this work, we focus on the formation of the feces cross section, which involves four faces out of the six. We hypothesize that the axial length of the cubes is set by mechanical drying instabilities. As lava cools, it shrinks, generating stress in the material. This stress is relieved if the lava cracks at regular intervals.[8] This is the mechanism underlying the formation of hexagonal columnar jointings and similar structures in drying corn starch cakes. While hexagons have been observed in these planar surfaces, and radial cracks have been observed in a circular anulus,[28] the crack structure occuring in drying cylinders remains unknown. Our preliminary work on drying corn starch suggests that lateral flat cuts as observed in wombat feces is one possibility, and may account for the remaining two faces of the cube.

The significance of cubic feces in evolution is ripe for future work, and we suggest some potential directions here. It is well known that wombats deposit aggregations of feces on prominent surfaces, such as rocks or logs, as exemplified in Fig. 1b, and it is widely hypothesized that their cubic shape facilitates the feces remaining on the surface. In preliminary tests, we explored the ability of cubic feces to prevent rolling and bouncing. We formed balls of dough in the same shape and size of wombat feces and dropped them from a height of 20 cm, comparable to the height of an adult wombat anus. When the feces landed on flat surfaces, cubes travel farther than spheres. When dropped onto inclined surfaces of $8°$, cubes end up 20 cm closer to the original impact site than spheres on average. Similar such tests could easily be done with natural substrates.

It is possible that the feces' cubic shape increases the surface area so that it can facilitate olfactory communication. Elevated scent-marking is a common behavior in many mammals and is hypothesized to increase scent dispersal and visibility.[29,30] The purpose of scent-marking is typically territorial,[30,31] however there is evidence that feces are also used in social communication[32] or communicating reproductive status.[33]

4 Conclusion

In this study, we show that wombats form corners in their feces using intestinal contractions coupled with the unique non-uniform material properties of their intestines. The questions of how and why wombats form cubic feces make up a compelling case study of the intersections between physiological, behavioral, and evolutionary ecology. However, they also have value in a range of other fields, particularly as a novel method of cube formation in manufacturing, and clinical pathology insight into the effect of human illnesses changing the tensile properties of the intestinal tract.

5 Materials and methods

Wombat tissues and fecal samples are all obtained from humanely euthanized individuals that were the victim of vehicle collisions. In this study, we present data from 3 wombat dissections. All dissections are performed after the specimen is frozen and thawed. In 2018, we dissect a young female wombat (2–3 years old). In 2019, we dissect an adult male wombat (>2 years old). And in 2020, we dissect a young male wombat (<2 years old).

5.1 Histology

We perform E&H staining on tissue samples taken every 1 cm along the entire circumference of both the proximal and distal colons. This sampling and staining was performed 3 times for

both the proximal and distal colons at locations separated by 1 cm axially in their respective regions. Sections were cut at thicknesses of 14 to 19 microns. The staining allows for the visual identification of the four major tissue layers: mucosa, glandular layer, circular muscle, and longitudinal muscle. We measured the thickness of each layer underneath a microscope using NIS-Elements software (see Table S1, ESI†).

5.2 Dryness testing

We evaluate fecal water content in the lower proximal colon (2–2.5 m from the anus) and distal colon (0–0.5 m from the anus). Five representative pieces of fecal material are extracted from the distal colon (all pieces are formed and distinct cubes) and two from the proximal colon (pieces not distinct, derived from the continuous slurry), they are weighed, dried at 60 °C until they no longer changed in mass (96 hours) and then re-weighed.

5.3 Tensile testing

The cut is made at a 50 cm distance from the anus. To measure the local stiffness at different azimuthal locations, we laser-cut a stencil to draw tick marks every 4 mm along the circumference of a 5 cm long tissue sample of proximal and distal colon. A ZXUEZHENG surgical marker (0.5 mm, from Amazon) provides the most visible tick marks. Two such rows are drawn 1 cm apart on each sample. To perform the tensile test, the sample is cut longitudinally.

Both ends of the cut tissue are clamped down with custom-made clamps (see Fig. 3e). Each clamp is made from laser-cut acrylic with sandpaper hot-glued to the inside, preventing the tissue from slipping. From one clamp, the sample is hung off a rod, while the bottom of a disposable water bottle is hung off of the bottom clamp. The sample is stretched by adding increments of water to the bottle. The clamp and bottle weigh 51.6 g. The sample is stretched by adding water to the bottle, a total of 7 times, in 25 ml increments. The sample is allowed to settle before the next increment of water is added. The test is recorded and we use the video labeler app from the Computer Vision toolbox in MATLAB to track the location of the interior end of the left row of tick marks. To get a full 360° test of the sample, 2 adjacent samples are prepared and the longitudinal cut is performed 180° offset of the other, allowing us to test regions of the tissue that would otherwise be covered by the clamps. A video of the test is shown in Video S3 (ESI†). Linear regressions of the local tensile data are shown in Fig. S1 and S2 (ESI†).

As shown in Fig. 3f, the first sample is denoted by blue dots while the other is denoted by red diamonds. The black line shows an averaging between the two samples at that azimuthal location, ignoring the edge-most data points of both samples due to edge effects from clamping down on the tissue.

5.4 Solving the equilibrium model

The intestine simulation does not attempt to model the non-Newtonian nature of the feces itself. Instead it represents the feces phenomenologically as increased damping and mass, aggregated at the intestinal walls. Without the feces, the nodes

may take on conformations that allow the springs to cross themselves in 2D space, which is not physically possible in the biological system. We find that using the equilibrium solution as the initial state helps prevent intersection of nodes during the contraction simulation.

The wombat intestines are modeled by a ring of springs (see Fig. 4a). The equilibrium shape is described by the length of the springs in the soft region l_A, the length of the springs in the stiff region l_B, the angles between the springs in the soft and stiff regions, ϕ_A and ϕ_B respectively, and the angle at the interfacial nodes between the stiff and soft regions ϕ_{AB}. A constant pressure, P, is exerted outwards on the nodes until the springs come to an equilibrium length. To solve for 5 unknown values, we require a system of 5 equations. Four of the equations come from local force balances: parallel to the angular bisector in the soft region (see eqn (5) and Fig. 4b) and the stiff region (see eqn (6)), and for the interfacial node, both parallel and perpendicular to the angular bisector (see eqn (7) and (8)). The equilibrium shape forms a convex $4n$-gon requiring the summation of the angles to be $\pi(4n - 2)$ (see eqn (9)).

$$\tan(\phi_A/2) = \frac{8nk(l_A - l_0)}{Pl_A} \tag{5}$$

$$\tan(\phi_B/2) = \frac{8Cnk(l_B - l_0)}{Pl_B} \tag{6}$$

$$\tan(\phi_{AB}/2) = \frac{8nk(l_A + Cl_B - (C + 1)l_0)}{P(l_A + l_B)} \tag{7}$$

$$\tan(\phi_{AB}/2) = \frac{P(l_B - l_A)}{8nk(l_A - Cl_B + (C - 1)l_0)} \tag{8}$$

$$\pi(4n - 2) = 2(n - 1)(\phi_A + \phi_B) + 4\phi_{AB} \tag{9}$$

In eqn (5)–(9), n is the number of nodes in each of the 4 sections of the ring, l_0 is the resting spring length, k is the base spring stiffness, and C is the spring stiffness ratio between the stiff and soft regions.

The equilibrium shape is numerically calculated using the MATLAB function fsolve. Both options MaxIterations and MaxFunctionEvaluations are set to 10^8. Each of the 4 regions are composed of $n = 50$ nodes as increasing n greater than 50 did not seem to change the resulting shape. The following are the parameters used in the default simulation. The unstretched length of every spring is $l_0 = 2\sin\left(\frac{\pi}{4n}\right)$, resulting in an unstretched ring of radius $R_0 = 1$ cm, matching the unstretched radius of the wombat's distal colon. The base spring stiffness is $k = 0.1 \times 10^4$ g s^{-2}, and the stiffness of each spring was $4nk$ and $4Cnk$ for the soft and stiff springs respectively. The spring stiffness ratio is $C = 4$. Multiplying the spring stiffness by $4n$ normalizes the overall stiffness of the ring to be independent of the number of nodes used in the simulation and results in the softer spring stiffness to be equivalent to 0.2 N mm^{-1} as found from tensile testing. The function fsolve requires an initial

guess at the solution, $(l_A, l_B, \phi_A, \phi_B, \phi_{AB}) = (l_0 + 10^{-4}, l_0, (4n - 2)\pi/(4n), (4n - 2)\pi/(4n), (4n - 2)\pi/(4n))$.

The simulation fails to run if the equilibrium solution cannot be found. This may happen when the spring stiffness ratio C is too close to 1. When $C = 1$ the system is over-constrained and, as described to the MATLAB function fsolve, cannot find the equilibrium solution. We find this happens when $C < 2$. MATLAB may also fail to find the equilibrium solution if k is too high. This may be due to eqn (5)–(8) holding too much weight, not allowing fsolve to find a solution that also satisfies eqn (9). Due to this constraint, we measure all masses in units of 10^4 g, to keep $k < 1$.

5.5 Simulating the model intestine contractions

The contraction is simulated by solving the equations of motion according to Newton's second law, $F = ma$, eqn (10). Each node is subject to two neighboring spring forces and a damping force.

$$m\dot{\vec{v}}_i = k_i(\|\vec{x}_{i+1} - \vec{x}_i\| - l_0)(\widehat{x_{i+1} - x_i})$$
$$+ k_{i-1}(\|\vec{x}_{i-1} - \vec{x}_i\| - l_0)(\widehat{x_{i-1} - x_i}) - b\vec{v}_i. \quad (10)$$

where $\|\vec{u}\|$ indicates the magnitude of vector u and $\hat{u}$ means that vector u is scaled to be a unit vector. We close the system with the definition of velocity,

$$\vec{v}_i = \dot{\vec{x}}_i \quad (11)$$

The differential equation is solved over a time period of $t = [0, 40 \text{ s}]$ using the MATLAB function ode45. For simulations involving changes in damping, the simulation time is extended linearly as damping is increased, according to $t_f = 10^5 b$, where t_f is the duration of the simulation, and b is the damping coefficient. The equilibrium solution is used to get the initial xy coordinates of all $4n$ nodes and their initial velocities are set to 0.

The following are the parameters for the default simulation. The added mass of each node is set to $m = 4.5 \times 10^{-6} \ 10^4$ g. This mass is calculated by multiplying our 2D density of feces, $\rho_{2D} = 1$ g cm^{-2} by the equilibrium mean radius squared, R^2, then dividing by the number of nodes. Recall that mass must be measured in units of 10^4 g to keep the base spring stiffness k low. The damping coefficient is set to be $b = 4.5 \times 10^{-3} \ 10^4$ g s^{-1}. To contract the system, the rest length of the springs is decreased, from l_0 to $l_0/4$. The system oscillates as a square wave between l_0 and $l_0/4$ with a period $\tau = 1$ s. Over the simulation time, this period results in 40 simulated oscillations and Re = 10^{-3}.

5.6 Calculating curvature

The shape of the simulation is analyzed by calculating the curvature at 20 azimuthal positions. Nodes from the simulation are translated so that the center is located at (0,0). They are then binned together according to their θ location in polar coordinates. While in polar coordinates, the points are rotated so that the center of the bin is at $\theta = \pi/2$. The points are mapped backed to Cartesian coordinates so that we may fit a degree 2 polynomial $y = f(x)$ to the points. From the polynomial, the average curvature of those points is calculated according to eqn (12).

$$
\begin{aligned}
\kappa_{\text{avg}} &= \frac{1}{x_{\max} - x_{\min}} \int_{x_{\min}}^{x_{\max}} \frac{f''(x)\mathrm{d}x}{(1 + f'(x)^2)^{3/2}} \\
&= \frac{1}{x_{\max} - x_{\min}} \left| \frac{f'(x_{\max})}{\sqrt{1 + f'(x_{\max})^2}} - \frac{f'(x_{\min})}{\sqrt{1 + f'(x_{\min})^2}} \right|
\end{aligned}
\quad (12)
$$

5.7 Quantifying squareness

The wombat feces themselves are not perfect cubes, as the corners, while distinct, are clearly rounded. There exist several metrics for measuring a shape's roundness.[24] For measuring squareness, we found a single existing metric called the squircle.[25] Attempts to use it on our biological data showed that it was not robust to noise (see more discussion in the ESI†). We propose a new metric to evaluate squareness S which comes from comparing the measured curvature $\kappa(\theta)$ to a reference curvature signal.

When considering the reference curvature signal, note that a circle displays constant curvature for all values of θ, while a square has $\kappa(\theta) = 0$ for all values of θ except $\kappa(\theta) = \infty$ at each of the 4 corners. The template for our reference signal is then based upon the following impulse function

$$f_\lambda(x) = \frac{1}{\lambda}e^{-|x|/\lambda}. \quad (13)$$

We can check the validity of this equation by considering the limit as λ tends to infinity: $\lim_{\lambda \to \infty} f_\lambda(x) = $ constant, behavior which is similar to the curvature signal of a circle. Likewise, for the limit as λ tends to zero, $\lim_{\lambda \to 0} f_\lambda(0) = \infty$ and $f_\lambda(x|x \neq 0) = 0$, similar to the curvature signal around a single corner of a square. We will use λ to describe the sharpness of a shape's corners. This impulse function also has the added benefit that the area under the curve is constant for all λ.

$$\int_{-\infty}^{\infty} \frac{1}{\lambda}e^{-|x|/\lambda}\mathrm{d}x = 2 \quad (14)$$

We use this property to scale the function based on the size of the shape. For a circle with area A

$$\kappa_{\text{circle}}(\theta) = \sqrt{\frac{\pi}{A}} \quad \int_0^{2\pi} \kappa_{\text{circle}}(\theta)\mathrm{d}\theta = 2\pi\sqrt{\frac{\pi}{A}}. \quad (15)$$

We may then scale our reference curvature signal for any arbitrary shape such that the area under the curve is $2\sqrt{\frac{\pi^3}{A}}$.

To match the 4 peaks in curvature that a square displays, we express the curvature as a piece-wise function, mapping the original infinite domain to a finite one. In doing so, our function's area under the curve is no longer conserved over λ. We remedy this by scaling by the integrated area under the curve, from zero to $\pi/2$, which is relevant for each of the pieces

of the piecewise function. Overall we have

$$\kappa_{\text{ref}}(\theta,\lambda) = \frac{\sqrt{\frac{\pi^3}{A}}\left(\frac{1}{\lambda}e^{-|\tan(\theta-\psi)/\lambda|}\right)}{\int_0^{\pi/2}\frac{1}{\lambda}e^{-\tan\tilde{\theta}}d\tilde{\theta}} \quad (16)$$

where

$$\psi = \begin{cases} \pi/4 & \theta \in (0,\pi/2) \\ 3\pi/4 & \theta \in (\pi/2,\pi) \\ 5\pi/4 & \theta \in (\pi,3\pi/2) \\ 7\pi/4 & \theta \in (3\pi/2,2\pi) \end{cases}$$

The reference function displays discontinuities at $\theta = \frac{n\pi}{2}$, $\forall n \in \mathbb{Z}$. From κ_{ref}, we inherently get the first component of our squareness metric in λ, in which high values of λ indicate the shape is very circular, while values close to 0 indicate the shape is square.

To match the measured $\kappa(\theta)$ to the proper value of λ, we cross-correlate the signals $\kappa(\theta)$ and $\kappa_{\text{ref}}(\theta,\lambda)$ using the xcorr function available in MATLAB (see Fig. 5a). Both signals must be sampled at the same values of θ. The measured $\kappa(\theta)$ is made continuous by linearly interpolating between values. The function xcorr finds the correlation between signals at varying lags, rotating the shape until the curvature signals are aligned. When performing the cross-correlation, we input three periods of each curvature signal, $\theta = [0,6\pi]$ and specify that the lag may not be more than 2π. This prevents xcorr from correlating to different signals by only comparing a small part of each signal. We numerically find the value of λ that yields the maximum correlation x using MATLAB's built-in fminsearch and an initial guess of $\lambda = 1$. With the optimal value for λ and the corresponding correlation x, we calculate squareness as

$$S = x^{10}(1 - 2\arctan(\lambda)/\pi). \quad (17)$$

The range of S is $(0,1)$ where $S = 1$ indicates that the shape is perfectly square, and $S = 0$ indicates that the shape is either perfectly circular or very much not square. The correlation, x, is raised to the 10th power. This exponent weights the correlation to ensure that the shape is given a high score only when it has 4 peaks in curvature rather than just 2 very high peaks in curvature. In practice, 2 high peaks in curvature may result in a correlation of $x \approx 0.9$. Raising the correlation to the 10th power sufficiently punishes these non-square shapes.

We illustrate the evaluation of squareness with a numerical example. Consider a single frame at $t = 7.9$ s from the square simulation using the default parameters listed above ($C = 4$, $m = 4.5 \times 10^{-6}$ 10^4 g, $b = 4.5 \times 10^{-3}$ 10^4 g s^{-1}). The function ode45 gives the xy coordinates of all n nodes at each time point. From these coordinates, we calculate curvature κ using eqn (12) for each bin of nodes. We then get a function $\kappa(\theta)$ for any arbitrary value of θ by linearly interpolating between calculated curvature values. We sample the curvature $\kappa(\theta)$ every 0.6° (0.1 radians) from 0.6° to 359.4°. The resulting vector of curvature values is then repeated 3 times so that cross-correlation by the function xcorr will not be inflated by comparing too few data points.

Using the function fminsearch we compare the curvature $\kappa(\theta)$ to the reference curvature $\kappa_{\text{ref}}(\theta,\lambda)$ as described by eqn (16), sampling at the same values of θ, searching for the value of λ that yields the highest cross-correlation. For $t = 7.9$ s, this optimal value is $\lambda = 1.5$ with a cross-correlation of $x = 0.98$. Fig. 5a shows the curvature from the simulation (solid black line) as well as the reference curvature $\kappa_{\text{ref}}(\theta,\lambda = 1.5)$ (dotted blue line). The range of λ is $(0,\infty)$, so we map λ to a range $(0,1)$ with 1 indicating highest squareness and multiply it with the cross-correlation value x^{10} as in eqn (17). The resulting mapping, from eqn (17) yields a squareness of $S = 0.3$. We repeat this procedure for every time increment in the contraction.

Ethics

For the CT-scanning, Animal Ethics approval was sought and granted by the Taronga Conservation Society Australia (protocol number 3e0419).

Author contributions

PY, AL, DH, SC contributed to the conception or design of the work; AL, MC, MK, KQ, CW, LV, AM, AE, SC, DH to the acquisition, analysis, or interpretation of data; AL, GC, MB, BM to the creation of new software used in the work; AL, SC, DH have drafted the work and substantively revised it.

Conflicts of interest

There are no conflicts to declare.

Acknowledgements

References

1 E. R. Guiler, *Marsupials of Tasmania. The Trustees of the Tasmanian Museum and Art Gallery*, 1960, available from: https://trove.nla.gov.au/version/33491769.

2 D. T. Gwynne, K. M. O'Neill and W. L. Rubink, The Evolutionary Significance of Fusiform Feces: A Predator-Prey

Model, *The Worm Runner's Digest*, 1978, vol. 20(iss. 1), pp. 91–92.

3 B. Triggs, *Wombats*, CSIRO Publishing, Australia, 2nd edn, 2009.

4 J. Woodford, *The Secret Life of Wombats*, 2012. Google-Books-ID: fg_KIKj7fXsC.

5 J. French, *The Secret World of Wombats*, HarperCollins Publishers, Pymble, Sydney NSW, Australia, 2005.

6 P. J. Yang, M. LaMarca, C. Kaminski, D. I. Chu and D. L. Hu, Hydrodynamics of defecation, *Soft Matter*, 2017, **13**(29), 4960–4970. Available from: http://xlink.rsc.org/?DOI= C6SM02795D.

7 T. Takahashi, Flow Behavior of Digesta and the Absorption of Nutrients in the Gastrointestine, *J. Nutr. Sci. Vitaminol.*, 2011, **57**(4), 265–273. Available from: https://www.jstage.jst.go.jp/article/jnsv/57/4/57_4_265/_article.

8 L. Goehring, L. Mahadevan and S. W. Morris, Non-equilibrium scale selection mechanism for columnar jointing, *Proc. Natl. Acad. Sci. U. S. A.*, 2009, **106**(2), 387–392. Available from: http://www.pnas.org/cgi/doi/10.1073/pnas.0805132106.

9 H. C. Jensen, Production of Chladni Figures on Vibrating Plates Using Continuous Ex-citation, *Am. J. Phys.*, 1955, **23**(8), 503–505. Available from: http://aapt.scitation.org/doi/10.1119/1.1934080.

10 C. Ellegaard, A. E. Hansen, A. Haaning, K. Hansen, A. Marcussen and T. Bohr, *et al.*, Creating corners in kitchen sinks, *Nature*, 1998, **392**(6678), 767–768. Available from: https://www.nature.com/articles/33820.

11 J. W. M. Bush, J. M. Aristoff and A. E. Hosoi, An experimental investigation of the stability of the circular hydraulic jump, *J. Fluid Mech.*, 2006, **558**, 33. Available from: http://www.journals.Cambridge.org/abstract_S0022112006009839.

12 S. R. Jongerius and D. Lentink, Structural Analysis of a Dragonfly Wing, *Exp. Mech.*, 2010, **50**(9), 1323–1334, DOI: 10.1007/sll340-010-9411-x.

13 M. Burrows and G. Sutton, Interacting Gears Synchronize Propulsive Leg Movements in a Jumping Insect, *Science*, 2013, **341**(6151), 1254–1256. Available from: http://science.sciencemag.org/content/341/6151/1254.

14 P. S. Barboza, Digestive Strategies of the Wombats: Feed Intake, Fiber Digestion, and Di-gesta Passage in Two Grazing Marsupials with Hindgut Fermentation, *Physiol. Zool.*, 1993, **66**(6), 983–999. Available from: http://www.jstor.org/stable/30163750.

15 P. S. Barboza and I. D. Hume, Digestive tract morphology and digestion in the wombats (Marsupialia: Vombatidae), *J. Comp. Physiol., B*, 1992, **162**(6), 552–560. Available from: http://link.springer.com/10.1007/BF00264817.

16 G. Hounnou, C. Destrieux, J. Desm, P. Bertrand and S. Velut, Anatomical study of the length of the human intestine, *Surg. Radiol. Anat.*, 2002, **24**(5), 290–294, DOI: 10.1007/s00276-002-0057-y.

17 K. Milton and M. W. Demment, Digestion and Passage Kinetics of Chimpanzees Fed High and Low Fiber Diets and Comparison with Human Data, *J. Nutr.*, 1988, **118**(9), 1082–1088. Available from: https://academic.oup.com/jn/article/118/9/1082/4739307.

18 M. Evans, B. Green and K. Newgrain, The field energetics and water fluxes of free-living wombats (Marsupialia: Vombatidae), *Oecologia*, 2003, **137**(2), 171–180, DOI: 10.1007/s00442-003-1322-4.

19 A. M. Martin, T. A. Fraser, J. A. Lesku, K. Simpson, G. L. Roberts and J. Garvey, *et al.*, The cascading pathogenic consequences of Sarcoptes scabiei infection that manifest in host disease. Royal Society Open, *Science*, 2018, **5**, 180018.

20 C. N. Johnson, The evolutionary ecology of wombats, in *Wombats'*, ed. R. T. Wells and P. A. Prid-more, 1998, pp. 34–41.

21 R. T. Wells and P. A. Pridmore, of South Australia RZS, ed. Wombats. Norton, N.S.W: Surrey Beatty and Sons in association with the Royal Zoological Society of South Australia; 1998, OCLC: 41666093.

22 R. G. Lentle and P. W. M. Janssen, Physical characteristics of digesta and their influence on flow and mixing in the mammalian intestine: a review, *J. Comp. Physiol., B*, 2008, **178**(6), 673–690, DOI: 10.1007/s00360-008-0264-x.

23 S. M. Woolley, R. S. Cottingham, J. Pocock and C. A. Buckley, Shear rheological properties of fresh human faeces with different moisture content, *Water SA*, 2014, **40**(2), 273–276. Available from: https://www.ajol.info/index.php/wsa/article/view/102220.

24 J. W. Bullard and E. J. Garboczi, Defining shape measures for 3D star-shaped particles: Sphericity, roundness, and dimensions, *Powder Technol.*, 2013, **249**, 241–252. Available from: http://www.sciencedirect.com/science/article/pii/S0032591013005263.

25 M. Fernandez Guasti, Analytic geometry of some rectilinear figures, *Int. J. Math Educ. Sci. Technol.*, 1992, **23**(6), 895–901. Available from: https://luz.izt.uam.mx/mfg/arti/90-94/agrec-ijmest92.pdf.

26 S. K. Sarna, Colonic Motility: From Bench Side to Bedside, *Integrated Systems Physiology: From Molecule to Function to Disease*, Morgan Sz Claypool Life Sciences, San Rafael (CA), 2010. Available from: http://www.ncbi.nlm.nih.gov/books/NBK53477/.

27 D. Xu, A. Varshney, X. Ma, B. Song, M. Riedl and M. Avila, *et al.*, Nonlinear hydrodynamic in-stability and turbulence in pulsatile flow, *Proc. Natl. Acad. Sci. U. S. A.*, 2020, **117**(21), 11233–11239. Available from: https://www.pnas.org/content/117/21/11233.

28 M. M. Bandi, T. Tallinen and L. Mahadevan, Shock-driven jamming and periodic frac-ture of particulate rafts, *EPL*, 2011, **96**(3), 36008. Available from: http://stacks.iop.org/0295-5075/96/i=3/a=36008?key=crossref.C43803f2f557d0389ad41abf7d09b71e.

29 D. W. Macdonald, Patterns of Scent Marking with Urine and Faeces Amongst Carnivore Com-munities, *Symposium of Zoological Society London*, 1980, **45**, 107–139.

30 I. Barja and R. List, Faecal marking behaviour in ringtails (Bassariscus astutus) during the non-breeding period: spatial characteristics of latrines and single faeces, *Chemoecology*, 2006, **16**(4), 219–222, DOI: 10.1007/s00049-006-0352-x.

31 K. Kilshaw, C. Newman, C. Buesching, J. Bunyan and D. Macdonald, Coordinated Latrine Use by European Badgers, Meles meles: Potential Consequences for Territory Defense, *J. Mammal.*, 2009, **90**(5), 1188–1198. Available from: https://academic.oup.com/jmammal/article/90/5/1188/873428.

32 C. Marneweck, A. Jrgens and A. M. Shrader, The role of middens in white rhino olfactory communi-cation, *Anim. Behav.*, 2018, **140**, 7–18. Available from: http://www.sciencedirect.com/science/article/pii/S000334721830109X.

33 C. E. Merte, T. E. Goodwin and B. A. Schulte, Male and female developmental differences in chemosen-sory investigations by African elephants (Loxodonta africana) approaching water-holes, *Behav. Ecol. Sociobiol.*, 2010, **64**(3), 401–408. Available from: http://link.springer.com/10.1007/s00265-009-0856-9.